

Effect of geometry variation on the mechanical behavior of the proximal femur

ABSTRACT:

The mechanical behavior of a proximal femur under a normal body weight loading was examined. The geometry of the proximal femur was created in a finite element model using 29 reference points measured on the CT scan images of a patient. Four additional sets of measurements were calculated using $\pm(1)$ and $\pm(2)$ the standard deviation of the original set and the result of models was compared. The stress distribution and the locations of critical normal and shear stress, as well as the effect of the femur geometry which may be most susceptible to failure were examined. The findings of this study demonstrate an inferior distribution of stress in the plus-standard deviation models and also indicate less ability to bear weight. The minus-standard deviation models appear to be better suited to bearing weight and indicate a more even distribution of the stresses generated within the proximal femur.

Keywords: proximal femur, stress distribution, geometry, standard deviation, finite element analysis

1. INTRODUCTION

The evolution of a human into an upright, two-legged being has lead to the hip and lower limbs becoming the chief weight-bearing structures. Activities such as running and jumping involve high impact forces that generate further stress in the bones of the lower limb, in addition to those caused by the load of normal body weight [1].

The femur serves as a powerful lever, transmitting large magnitudes of load essential to everyday movement. It is the largest and longest bone and in the human body [2] and can be divided into the diaphysis (shaft) and the articular surfaces at each end.

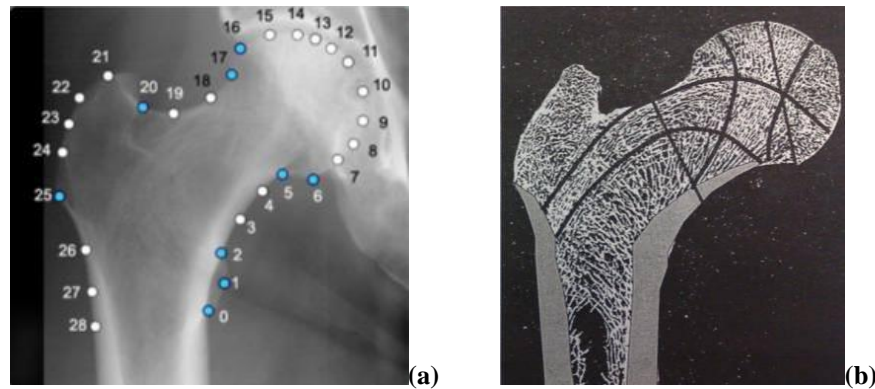
The shaft of the femur is basically a tubular structure made up of a thick layer of dense, compact bone tissue (cortical bone) that surrounds a hollow cavity known as the medullary cavity. Towards the proximal femur, the thickness of the cortical bone quickly decreases. The space within the proximal femur is replaced by cancellous bone arranged in a complex lattice structure, known as the trabeculae. The trabeculae can be divided into two systems: the principal compression system and the principal tension system [2, 3], as seen in Fig. 1.

Studies on the femur have been made that show an overall compression in the bone [4, 5]. Rudman et al. [6] go a step further to examine the stress distribution in the proximal, where they hypothesize that the proximal femur is mainly in compression under physiological loading, and their results support this hypothesis.

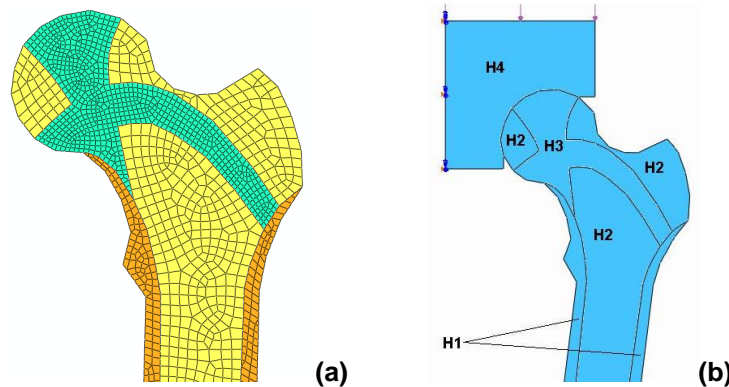
37 The objective of this study is to expand on the work of Rudman et al. [6], which makes use of a single average model.
38 However, as the geometry and material properties (such as the apparent density of bone tissue) of the femur may change
39 due to age, nutritional status or bone disease. The ensuing study examines how the stress distribution in the proximal
40 femur may change with relative geometry. It will also attempt to identify the locations of maximum normal and shear
41 stress, as well as the areas and geometries, which may be most susceptible to failure.
42

43 2. MATERIAL AND METHODS

44
45 The original model used in this case was based on the CT scan images of a single individual (gender and age were
46 undisclosed). Twenty-nine reference nodes were defined on the proximal femur for the subsequent measurements. Four
47 additional sets of measurements were calculated using $\pm(1)$ and $\pm(2)$ the standard deviation of the original set. The finite
48 element (FE) software, Abaqus 6.7 (Simulia Dassault Systèmes), was used to build and analyze the simulation models.
49 The resulting models are named according to their deviation from the original model ((0)-model). In total, 5 models (0, -1, -
50 2, +1 and +2 models) created and were used in the ensuing study.
51



52
53 **Fig. 1. Coordinate geometry for the proximal femur (Provided by the Division of Applied Medicine, University of**
54 **Aberdeen) (a); pattern of trabeculae within proximal femur [6] (b).**
56



57
58 **Fig. 2. The finite element model created based on the measured geometry and proposed pattern of the proximal**
59 **femur (a); partition of the proximal femur based on the pattern of tension-compression presented in Fig 1 (b).**
60
61

62 For all the models, the bone is partially reconstructed. The model includes a representative section of the acetabulum and
63 labeled “H4” (Fig. 2). The distal femur that includes the knee area has been excluded in the modeling. For stability and
64 more accurate rendering of the bone’s deformation under loading, an arbitrary length of the shaft is included. The cortical
65 bone surrounding the femoral shaft is assigned a density of 2.2 g/cc [7], Young’s modulus of 17GPa, and Poisson’s ratio
66 of 0.33 [4, 6].
67

68 The internal structure of the models is partitioned (Fig. 2), as defined by Rudman et al. [6], following the lines of stress in
69 the bone trabeculae. The principal compression and principal tension groups (Fig. 1) are represented as a single part
70 labeled “H3” in the FE model (Fig. 2). This part was given Young’s modulus of 400MPa [6]. Density and Poisson’s ratio
71 remains the same as the cortical bone. The remaining surrounding trabeculae and cavity in the shaft (H2) are given a
72 modulus of 100 MPa [6] and apparent density of 1.2 g/cc from a range of values [8]. The acetabulum is assigned the

73 same material properties as the H3 trabeculae. Each part is assumed to be of homogeneous and isotropic material.
 74 Although true bone trabeculae have a lattice structure, it is challenging to recreate precisely. The assumptions should give
 75 a close enough representation and fairly good results [4, 5, 6, 9], in addition to making the simulations more comfortable
 76 to work with.

77
 78 The model is meshed using 4-node quadrilateral elements with reduced integration. As a 2-dimensional model, no
 79 thickness is assigned, and the model only undergoes linear plane stress in two directions. A finer mesh is assigned in the
 80 H3 part in order to obtain more precise results in the proximal femur.

81
 82 Boundary conditions are applied to replicate in vivo conditions as closely as possible (Fig 3). Part H4 is fixed only on the
 83 medial side. The distal end is pinned, as there should be zero-moment at the knee when weight is applied. The average
 84 body weight of 700N (70kg) is assumed. Further, assuming that bodyweight is uniformly distributed during the two-legged
 85 standing stance (the person is standing at rest), it is inferred that the load carried by each leg is 350N.
 86

87 3. RESULTS AND DISCUSSION

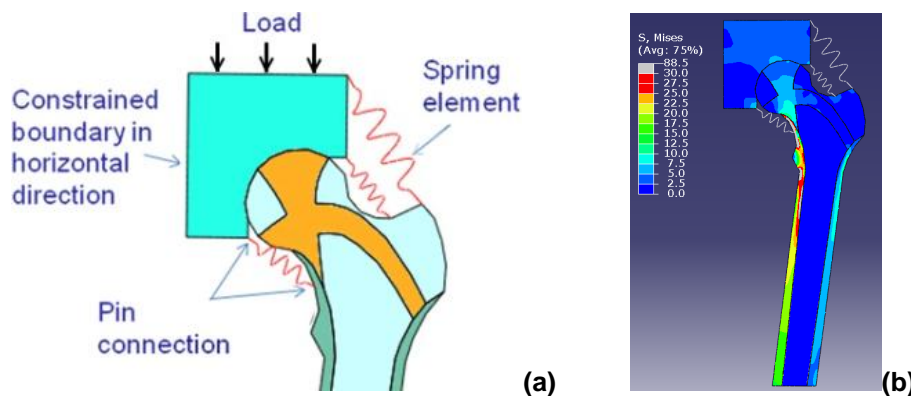
88 3.1 Deformation and displacement

89 When the load was applied, the models showed a deflection on the femoral head, together with a displacement in the
 90 lateral direction in by femoral shaft. These were the maximum displacements in the entire represented femur, and the
 91 location of these deflections remained unchanged throughout all models. The values of these displacements are shown
 92 below in Table 1.
 93
 94

95 Fig. 3 shows a typical femur model after the load was applied. Except for the case of the (+2)-model, the readings show
 96 displacement differing by about ± 2.0 mm from the (0)-model, which does not seem too unusual. The (+2)-model is the
 97 exception with an uncharacteristically large variance in values. With this in mind, we carry on to examine the normal and
 98 shear stress responses of the (0)-model and the standard deviation models.

99
 100 **Table 1. Maximum displacement (mm) values found in the femoral head and shaft**

Standard deviation	-2	-1	0	+1	+2
Displacement, femoral head	21.5	20.0	19.0	18.0	12.0
Displacement, shaft	26.9	25.0	24.8	23.0	17.0



104
 105 **Fig. 3. (a) loading and boundary conditions; (b) a typical stress distribution in an analyzed model. The colors**
 106 **show the level of stress on the bone.**

107 3.2. Normal & shear stress response

108 3.2.1. Mean/average model, (0)-model

109 Under the static 350N load, the bulk of the trabeculae is shown to be under stresses up to -1.1 kN/cm². A contour plot of
 110 normal stress reveals an area in part H3 under higher compression. The compression in this area appears to stem from
 111 the acetabulum and continues directly into the cortical bone of the medial shaft, which is under even higher compressive
 112
 113
 114
 115

116 stress. The compression in the proximal femur is most concentrated at a point in the superior head, with a value of -
117 6.4kN/cm². Maximum tensile stress in the proximal femur is output as +1.6kN/cm² and is located in a mesh element
118 directly below the maximum compression.

119 The output readings from the model show that the femur is mainly under negative shear stress. Negative shear found in
120 the proximal femur and acetabulum appears to be of relatively low magnitude, and the plot shows areas in the acetabulum
121 and the inferior femoral head that reach values up to -0.6kN/cm² to -0.94kN/cm². This is about 3x values found in the
122 surrounding trabeculae.

123 The largest shear values in the proximal femur are located in the superior femoral head. The maximum negative shear is
124 determined to be -1.7kN/cm² and is accompanied by a mesh element bearing the maximum positive shear (+1.8kN/cm²)
125 in the same part.

126 **3.2.2. Minus one (-1) standard deviation model**

127
128 The (-1)-model shows the trabeculae to be under compressive stresses between -0.88kN/cm² to -2kN/cm², the contour
129 plot appearing to suggest a more uniform distribution of stresses. The large area of higher compression in the femoral
130 head, as seen during the (0)-model simulation, does not appear in the plot for the (-1)-model. However, there is evidence
131 that a similar pattern of behavior may emerge. The result shows a small cluster in the inferior femoral neck in a higher
132 range of compression than its surroundings; this connects to the medial cortical bone that is also in comparatively high
133 compression. The maximum compression in the proximal femur is also shown to be located in the superior femoral head,
134 although it is smaller in magnitude at -6.0kN/cm².

135 Within the greater trochanter, the trabeculae appear to be in mild tension. The H3 part trabeculae experience a principal
136 tensile load and show tension growing towards the lateral metaphysis. The maximum tension (+1.1kN/cm²) in this model
137 is found here and is located right next to the cortical bone.

138 The metaphysis experiences relatively low positive shear. The most significant positive shear stress (+0.34kN/cm²) found
139 in the femoral neck is in the inferior, close to the cortical bone.

140 The negative shear found in this model mostly follows a similar trend of being relatively small in magnitude. The trend
141 breaks in the most inferior and superior sections of the head. The inferior femoral head shows negative shear stress in the
142 region of -1.0kN/cm² building up where the cortical bone starts to grow thicker. The superior proves to be the location of
143 both the maximum negative and maximum positive shear stresses. The values of which are -1.3kN/cm² and +1.6kN/cm²,
144 and their location corresponds to the location of maximum compression. The proximal femur is ultimately found to be
145 under net negative shear stress.

146 **3.2.3. Minus two (-2) standard deviation model**

147
148 The normal stress result of (-2)-model bears a close resemblance to the corresponding plot for the (-1)-model. In most of
149 the trabecular bone, the model registers compression values up to around -0.9kN/cm² to -1.8kN/cm². Similar to the (-1)-
150 -model, there is an area in the inferior neck under high-er compression leading into the cortical bone of the medial shaft.
151 The point of maximum compressive stress in the superior head is found to be -5.6kN/cm².

152
153 The maximum tension in the proximal femur is located in the lateral metaphysis and within the H3 part, similar to that seen
154 in the (-1)-model. The magnitude is also around +1.1kN/cm².

155 The result of shear stress for the (-2)-model shows most of the metaphysis to be under low positive shear stress, with a
156 maximum of +0.4kN/cm² found in the inferior neck, close to the cortical bone. Negative shear stress occurs in the
157 epiphysis, mainly in the inferior and medial. The maximum negative shear for the proximal femur is -1.4kN/cm², and is
158 found in the inferior femoral head. The location of maximum negative shear is different from the other models, virtually on
159 the opposite side. The maximum positive shear in the head reaches just under +1.0kN/cm², and its location remains
160 unchanged from other models. Negative shear is still generated next to this point but remains relatively low in magnitude
161 (-0.36kN/cm²).

162 Despite large areas of the proximal femur being under positive shear, the magnitudes are very low in comparison to the
163 small areas that are under much higher magnitudes of negative shear stress. This results in the proximal femur being
164 under net negative shear.

165 **3.2.4. Plus (+1&+2) standard deviation models**

166
167

168 The result of the normal stress in the (+1)-model looks almost identical to the (0)-model. The values in the field output
169 report of normal and shear stress indicate a shift towards tensile stress in the proximal femur. Despite this shift, the field
170 output shows that the net stress response in the proximal femur remains compressive and smaller in magnitude than the
171 (0)-model.

172 The location of maximum compression in the proximal femur remains in the superior femoral head and is found to be -
173 7.7kN/cm². This turned out to be the highest compression reading out of all the five models. In addition, the maximum
174 tensile stress (+2.5kN/cm²) in the proximal femur was found to be located close to the maximum compression. This is
175 similar to what was seen in the (0)-model response.

176 The shear stress for this model also bears a substantial similarity to the (0)-model. More or less the same areas have
177 been highlighted, although as with the normal stress response, the values show a fair amount of difference. The data
178 extracted show the magnitudes of both negative and positive shear increasing in the proximal femur. Despite this, the net
179 shear remains negative and is of lower magnitude. As well, part H3 demonstrates a net positive shear, although its value
180 is comparatively small.

181 The maximum negative and positive shear values (-2.4kN/cm²; +2.1kN/cm²) are found in the superior femoral head, as
182 with the (0) & (-1)-models. Similarly, besides being close in proximity to each other, these maximum shear stresses
183 coincide with the location of the maximum normal stresses.

184 The normal stress output values for the (+2)-model show it has the lowest range of response of the five models. Most of
185 the proximal femur is found to bear stresses of about -0.6kN/cm² to just below +1.0kN/cm².

186 This model continues to exhibit higher compression areas in the femoral head that continue into the cortical bone. The
187 result can be said to look most similar to the (-2)-model. There is no change in the location of the maximum compressive
188 and maximum tensile stresses of the proximal femur, and are found in the superior epiphysis. However, the maximum
189 compression decreases dramatically to -6.1kN/cm², falling below the (0)-model. The maximum tension is output as
190 +2.3kN/cm².

191 The shear stress result of the (+2)-model actually seems closer to those of the minus deviation models. It clearly shows
192 positive shear building up in the metaphysis (particularly nearer the greater trochanter).

193 The position of maximum shear in the proximal femur remains unchanged and is found in the superior head within part
194 H3. The maximum negative shear is found to be -2.0kN/cm², and the maximum positive shear is +1.7kN/cm². Despite the
195 negative shear having a higher magnitude, the proximal femur for this model ends up being in net positive shear, in part
196 due to a larger existence of high magnitude positive shear in part H3. In addition, it was found that the location of
197 maximum negative shear in the H2 part has migrated. In previous models, this point was located in the superior femoral
198 head, next to the maximum shear stresses of the entire proximal femur. In the (+2)-model, this migrates through the H2
199 part into the distal femoral shaft.

201 4. DISCUSSION

202
203 The degree to which the femoral head deflects downward (Table 1) resembles the findings of a previous study [4]. In our
204 case, the readings do not appear unusual until the (+2)-model. The minus-models demonstrate gradually increasing
205 displacement. The plus-models were thus expected to show similar behavior of gradual decrease in displacement.
206 Although the plus-models do show smaller displacements, the (+2)-model shows a sharper decrease in magnitude
207 despite the same amount of load. Considering the behavior of previous models and the shifts in external geometry, the
208 (+2)-model appears to show fairly less flexibility. This behavior may be indicative of anisotropic nature. It suggests that
209 this study's assumption that bone tissue is isotropic may be over-simplistic. While the isotropic material assumption can
210 be useful, it seems to only be applicable to a certain extent and is unlikely to give genuinely accurate results.

211 The results consistently show in all models that the proximal femur is under net compression during loading. The part H3
212 carries higher compressive stresses that are transmitted into the cortical bone, and that are consistent with the location of
213 the principal compression system in the trabeculae. This coincides with the findings of Taylor [4] and Rudman [6]. The
214 simulations conducted in this study also reveal the maximum point compression in the proximal femur is always located at
215 a point in the superior head and is generated within the compression system in part H3.

216 The maximum values of compressive, tensile, and shear (negative and positive) stress found in the entire proximal femur
217 of each model are shown in Table 2. In each case, the maximum is generated within the H3 trabeculae and almost always
218 found to occur in the same location of the superior femoral head. Exceptions are seen in the minus-models, where the
219 different locations are identified in square parentheses.

220
221
222

Table 2. Maximum normal & shear stress values in the proximal femur

Standard deviation model	-2	-1	0	+1	+2
Compression, kN/cm ²	-5.6	-6.0	-6.4	-7.7	-6.1
Tension, kN/cm ²	+1.1	+1.1	+1.6	+2.5	+2.3
Negative shear stress, kN/cm ²	-1.4	-1.3	-1.7	-2.4	-2.3
Positive shear stress, kN/cm ²	> +1.0	+1.6	+1.8	+2.1	+1.7

223
224
225
226

The output report from Abaqus shows net compression in the proximal femur decreasing through the models, gradually at first from the (-2)-model to the (0)-model. The decrease is sharper from the (0)-model onwards. The (+2)-model shows net compression values in the proximal femur that are between 2-3 times smaller than the (0)-model.

227
228
229
230

From the values in Table 2 and the output report, it appears that the proximal femur becomes more capable of distributing stress loads internally as the external geometry shifts towards a lower deviation. Although net compression is higher, the maximum compressive load decreases, and the position of maximum tension shifts from the medial to the lateral proximal femur.

231
232
233
234
235
236
237
238
239
240
241
242
243

In theory, the opposite should then be right in the plus-standard deviation models. This does happen in the (+1)-model, although to a much higher degree than expected. This hypothesis then fails in the (+2)-model. The maximum tension remains relatively high, and like its two immediate predecessors, it is located right next to the point of maximum compression. However the maximum compressive load itself suddenly decreases, along with net compression values. As with the differences in displacement, this atypical behavior points towards an anisotropic characteristic and also casts doubt on the assumption of linearelasticity. The sudden difference in readings from the (+2)-model may suggest that the model is less reliable under the current simulation. Also constant in the simulated models are the locations of the resultant maximum negative and positive shear stress in the proximal femur. The results show the locations of the maximum shear stresses (both negative and positive) coincide with the location of maximum compressive stress in the proximal femur. The (-2)-model is the exception, whereby the maximum negative shear, in this case, is found in the inferior femoral head instead of the superior. This area is also highlighted in the other models as a location subject to higher negative shear than the surrounding trabecular bone in the inferior epiphysis. Except for the (+2)-model, the simulations show net negative shear stress generated in the proximal femur.

244
245
246
247

The plus-models show larger values of shear, and the output report shows that in both cases, the trabecular bone within part H3 is under net positive shear. The magnitude is relatively low in the (+1)-model but is shown to be much higher in the (+2)-model. Extraction of the maximum shear values from part H2 and their locations in each model provide a better understanding of these behaviors. This is tabulated in Table 3.

248
249

Table 3. The maximum shear stresses in part H2

Standard deviation	-2	-1	0	+1	+2
Negative shear stress, kN/cm ²	-0.36	-0.40	-0.36	-0.37	-0.21
Positive shear stress, kN/cm ²	+0.40	+0.34	+0.34	+0.37	+0.26

250
251
252
253
254

In all cases, the maximum positive shear within this part is located in the inferior femoral neck, near where the cortical bone starts to thicken. A maximum negative shear is found in the superior head, close to the location of the maximum positive shear of the H3 part trabeculae. The (+2)-model is an exception. In this model, the maximum negative shear in the H2 part migrates from the trabeculae into the shaft. Presumably, the area made up of the medullary cavity.

255
256
257

This migration and the readings recorded in Tables 2 & 3 could imply that in this particular model, (i) some form of failure has occurred under the current simulated conditions or (ii) the femoral shaft has now become at risk of failure for the particular geometry. If failure is indeed the case, it is highly likely to have occurred in the superior femoral head.

258 Overall, the findings in this study demonstrate the poorer distribution of stress by the plus-standard deviation models and
259 seem to indicate that these have a weaker ability to bear weight. On the other hand, the minus-standard deviation models
260 seem better suited to bearing weight and indicate a more even distribution of the stresses generated within the proximal
261 femur.

262 Failure in the proximal femur seems most likely to occur in the superior femoral head, as the location of maximum
263 compression remains in this area throughout each of the simulated models. The (0)-and plus-models seem particularly at
264 risk since this is the location of maximum tension in these models as well. For the most part, the same can be said of the
265 maximum shear stresses found in each model. The (-2)-model may seem to be an exception to the rule since the
266 maximum negative shear shifts down to the inferior head and is no longer acting directly against the maximum positive
267 shear. However, it continues to lie along the principal compression system of the trabecular bone that appears to transmit
268 stress into the cortical bone. This may lead to failure that starts from the inferior head rather than the superior. This
269 observation may be supported by the presence of some higher compression and negative shear in this region throughout
270 all five models.

271 The model used in this study is a basic 2-dimensional representation of the femur. Currently, the study does not take into
272 account the forces generated by ligaments and the muscle surrounding the femur. It also excludes the effects of the
273 articular cartilage and synovial fluid that lies between the acetabulum and femoral head. The inclusion of these factors in
274 future studies will give a much more accurate rendition of results.

275 With a 2-dimensional model, the study can give a good approximation as to the behavior of the proximal femur under
276 loading, but cannot be truly accurate. A 3-dimensional model, especially one that includes the physiological factors
277 mentioned above, may give a better representation.

278 The trabecular bone in the proximal femur is actually a complicated mesh of lamellar bone tissue. The exact architecture
279 is difficult to determine and even more challenging to represent in a computer simulation, not to mention one that is only in
280 2-dimensions. Furthermore, the findings of this study, looking at spread of forces across the different models imply an
281 anisotropic behavior in bone tissue. This suggests that to avoid structural failure, the in vivo bone will adjust itself to deal
282 with the range of applied loading and the varying stresses generated within the femur [12, 13]. This supports Wolff's law,
283 which states that bone is laid down in response to the quantity and quality of the load experienced [3, 4, 10]. Future
284 simulations may have to take this adaptive remodeling into account.

285 **5. CONCLUSIONS**

286 The finite element simulations reveal the presence of more considerable compression and tension in the trabeculae that
287 were consistent with the areas defined as the principal compression and principal tension systems. Our findings support
288 the theory that trabecular bone in the proximal femur acts as a vehicle to transfer the bulk of the stress borne by the femur
289 into the more compact and dense cortical bone. The path of transmission is consistent with the lines of stress first drawn
290 by Meyer [3] and Wolff [11].
291
292

293 We see that when the load is applied, a similar pattern of deformation occurs (downwards on the femoral head and
294 outward in the direction of the femoral shaft), though of varying magnitude.

295 Interestingly, we have also located the presence of increased shear response in the superior aspect of the femoral head
296 and the inferior neck. These areas may contribute to structural failure in the proximal femur, such as in predisposition to
297 fractures, especially in cases where there is a decrease in bone density or repetitive injury.

298 The findings of this study suggest that bone is actually anisotropic in nature; and that the structure of trabecular bone
299 within the proximal femur may change with outer geometry or loading conditions..

300
301
302

303 **COMPETING INTERESTS**

304
305 Authors have declared that no competing interests exist.

306
307
308 **CONSENT (WHERE EVER APPLICABLE)**

309 No manuscripts will be peer-reviewed if a statement of patient consent is not presented during submission (wherever applicable).

310 This section is compulsory for medical journals. Other journals may require this section if found suitable. It should provide a statement to confirm that the patient has given their informed consent for the case report to be published. Journal editorial office may ask the copies of the consent documentation at any time.

311
312
313
314
315
316 Authors may use a form from their own institution or SDI Patient Consent Form 1.0. It is preferable that authors should send this form along with the submission. But if already not sent during submission, we may request to see a copy at any stages of pre and post publication.

317
318
319
320 If the person described in the case report has died, then consent for publication must be collected from their next of kin. If the individual described in the case report is a minor, or unable to provide consent, then consent must be sought from their parents or legal guardians.

321
322
323
324 Authors may use the following wordings for this section: "All authors declare that 'written informed consent was obtained from the patient (or other approved parties) for publication of this case report and accompanying images. A copy of the written consent is available for review by the Editorial office/Chief Editor/Editorial Board members of this journal."

325
326
327
328
329 **ETHICAL APPROVAL (WHERE EVER APPLICABLE)**

330
331 All authors hereby declare that "Principles of laboratory animal care" (NIH publication No. 85-23, revised 1985) were followed, as well as specific national laws where applicable. All experiments have been examined and approved by the appropriate ethics committee.

332
333
334
335 **REFERENCES**

- 336
337 1. Orkin, P.A., 1952, The Evolution of Bone as Tissue and Organ, British Journal of Nutrition 6, pp401-405
- 338 2. Gray, H., 1901, Gray's Anatomy, In: Pickering Pick, T., Howden, R., (eds.) Revised American Edition from 15th English Edition: The Classic Collector's 1997 Edition, (Bounty Books, NY)
- 339 3. Bullough, P.G., 1992, Atlas of Orthopedic Pathology with Clinical and Radiologic Correlations 2nd Edition (Gower Medical Publishing)
- 340 4. Taylor, M.E., Tanner, K.E., Freeman, M.A.R., Yettram, A.L., 1996, Stress and strain distribution within the intact femur: Compression or bending? Medical Engineering and Physics, 18, pp122-131
- 341 5. Rohlmann, A., Mössner, U., Bergmann, G., Kölbl, R., 1982, Finite element analysis and experimental investigation of stresses in a femur. Journal of Biomedical Engineering 4, pp241-246
- 342 6. Rudman, K.E., Aspen, R.M., Meakin, J.R., 2006, Compression or tension? The stress distribution in the proximal femur. BioMedical Engineering OnLine 5:12
- 343 7. Wirtz, D.C., Schiffers, N., Pandorf, T., Radermacher, K., Weichert, D. Forst, R., 2000, Critical evaluation of known bone material properties to realize anisotropic FE-simulation of the proximal femur. Journal of Biomechanics 33, pp1325-1330
- 344 8. Kabel, J., Odgaard, A., van Rietbergen, B., Huiskes, R., 1999, Connectivity and the elastic properties of cancellous bone, Bone 24, pp115-120
- 345 9. Duda, G.N., Heller, M., Albinger, J., Schulz, O., Schneider, E., Claes, L., 1998, Influence of muscle forces on femoral strain distribution, Journal of Biomechanics 31, pp841-846
- 346 10. Fetto, J., Leali, A., Moroz, A., 2002. Evolution of the Koch model of the biomechanics of the hip: clinical perspective. Journal of Orthopaedic Science 7, pp724-730
- 347 11. Jang, I.G., Kim, I.Y., 2008, Computational study of Wolff's law with trabecular architecture in the human proximal femur using topology optimization, Journal of Biomechanics 41, pp2353-2361.

360
361
362
363
364
365
366

12. Chang Ho Yu, Young Jun Piao, Kyung Kim and Tae Kyu Kwon, Characteristic Analysis of the Lower Limb Muscular Strength Training System applied with MR Dampers, Bio-Medical Materials and Engineering 24 (2014) 297–306
13. ZHANG Shu-xu, ZHOU Ling-hong, LIN Sheng-qu, YU Hui, ZHANG Guo-quan, WANG Rui-hao and QI Bing, 4D-CT reconstruction based on pulmonary average CT values, Bio-Medical Materials and Engineering 24 (2014) 85–94